J Ther Eng, Vol. 11, No. 1, pp. 254−269, January, 2025

Journal of Thermal Engineering
Web page info: https://jten.yildiz.edu.tr
DOI: 10.14744/thermal.0000917

Research Article

Synergy of non-uniform heat source/sink and variable thermal conductivity on stagnation point flow of Casson fluid over a convective stretching sheet

C. Arruna NANDHINI[1,*], S. JOTHIMANI[2], Ali J. CHAMKHA[3]

[1]*Department of Mathematics, Kumaraguru College of Technology, School of Foundational Sciences, Tamil Nadu, 641049, India*
[2]*Department of Mathematics, Government Arts College (Autonomous), Tamil Nadu, 641 018, India*
[3]*Kuwait College of Science and Technology, Faculty of Engineering, Doha District, 35004, Kuwait*

ARTICLE INFO

Article history
Received: 25 December 2023
Revised: 16 March 2024
Accepted: 17 March 2024

Keywords:
Casson Fluid; Convective Stretching Sheet; Non-Uniform Heat Source/Sink; Stagnation Point and Constructive/ Destructive Chemical Reaction; Variable Thermal Conductivity

ABSTRACT

A novel approach is formulated to scrutinize the stagnation point flow of chemically reacting Casson fluid past a convective stretching sheet. Additionally, the combined impact of a non-uniform heat source/sink and variable thermal conductivity on the fluid flow is examined. With the aid of a suitable similarity transformation, the governing partial differential equations are transmogrified into corresponding ordinary differential equations. bvp4c, an in-built technique of MATLAB, is implemented to acquire the numerical solutions. The appurtenant parameters that exert influence on the concentration distribution, temperature distribution, and velocity profile are depicted graphically. The effects of various physical parameters such as Casson fluid parameter, magnetic field parameter, Prandtl number, Schmidt number, Eckert number, Biot number, variable thermal conductivity parameter, non-uniform heat source/sink parameters and velocity slip parameter are shown in plots for several ranges of values. In a constrained scenario, the accuracy and validity of the numerical technique utilized are justified by analogizing the procured outcomes with the pre-existing results in the literature. The influence of pertinent parameters that regulate the Nusselt number, skin friction coefficient, and Sherwood number is presented in tabular form. An upsurge in the variable thermal conductivity parameter reduces the temperature for internal heat generation, but for internal heat absorption, it diminishes the temperature adjacent to the wall and skyrockets the temperature far away from the wall. This current study is of immediate interest in the field of the aerospace industry due to the indispensability of variable thermal conductivity in lunar soft lander technology.

Cite this article as: Nandhini CA, Jothimani S, Chamkha AJ. Synergy of non-uniform heat source/sink and variable thermal conductivity on stagnation point flow of Casson fluid over a convective stretching sheet. J Ther Eng 2025;11(1):254−269.

***Corresponding author.**
*E-mail address: arruna98@gmail.com, arrunanandhini.c.sci@kct.ac.in

This paper was recommended for publication in revised form by Editor-in-Chief Ahmet Selim Dalkılıç

INTRODUCTION

On account of their prominence in physiological fluid dynamics as well as in the study of industry and engineering, various scientists expatiated about the flow dynamics of stagnation point under different circumstances. Over the last few years, the evaluation of stagnation flow towards a stretching surface has primarily been under consideration with the stipulation that, on its own plane, it is presumed that the velocity with which the sheet stretches is proportionate to the distance from the stagnation point. Such flows past stretching sheets often occur in engineering processes. Knowledge of the stagnation flow assists in the design of thrust bearings and radial diffusers, drag reduction, transpiration cooling, as well as thermal oil recovery. Moreover, the production of polymer sheets by continuous extrusion stands as an exemplar for its application in the manufacturing industry. Crane [1] was the instigator who analytically obtained the closed-form similarity solution of two-dimensional flow, which is attributable to the stretching plate. This groundbreaking investigation by Crane [1] has fascinated many authors. One of them was Chiam [2], who synthesized the stagnation point fluid flow from the stretching plate problem. He concluded that the flow in the proximity of the stretching surface is similar to the distant inviscid fluid flow from the plate; inevitably, there is no development of a boundary layer. Analytically, the problem of quadratically stretching sheet was elucidated by Kumaran and Ramanaiah [3]. The definitive Crane problem [1] was interpreted in their study as an incompressible viscous fluid. Pioneering work in heat transfer analysis incorporating thermal radiation was carried out by Raptis [4]. A typical aspect of all the above-mentioned assessments is the presupposition that the conventional no-slip condition is adhered to by the flow field at the sheet. In certain situations, nevertheless, a partial slip boundary condition must be utilized as the assertion of no slip no longer holds. C. L. M. H. Navier was the one who first proposed this slip-flow condition more than a century ago, and such a slip condition has been utilized recently in fluid flow studies over coated and rough surfaces, permeable walls, slotted plates, and liquid and gas flows in microdevices. This motivated Andersson [5] to derive the solution of viscous partial slip flow across a stretching sheet analytically.

Mahapatra and Gupta [6] deduced that the outcomes were contrary to those of Chiam [2]. It was asserted by them that a viscous layer emerges close to the stretching surface, and the framework of the boundary layer in the vicinity of the stagnation point relies upon "the velocity ratio of the stretching surface to that of the frictionless potential flow." Paullet and Weidman [7] numerically deduced the stagnation-point solution of flow across a stretching sheet. In partial differential equations (PDEs) form, Wang [8] demonstrated the Navier-Stokes system for the stagnation flow. More specifically, numerous metallurgical procedures involve the process of cooling. This is achieved by drawing the continuous filaments or strips through a quiescent fluid; occasionally, stretching of these strips occurs during the drawing process. The cooling rate has a significant impact on the final product's qualities when copper wires are annealed and thinned. The cooling rate can be restrained, and the desired final products may be earned. This is achieved by pulling the strips in an electrically conducting fluid with the application of a magnetic field [9]. With these in mind, Ishak et al. [10] numerically enunciated the stagnation point flow with the incorporation of a magnetic field via the Keller-Box method. The prominence of stagnation point flow in the field of hemodynamics was emphasized by Misra et al. [11]. The model proposed by them not only finds applications in species separation and drug delivery but also stands as a complement to studies on microcirculatory systems. Under the existence of a heat source/sink, heat transfer across a stretching sheet on MHD stagnation point flow was analyzed by Agbaje et al. [12]. In their survey, results were procured by employing the Chebyshev spectral method-based perturbation technique and the Spectral Quasi-Linearization Method (SQLM). Further, it is figured out that the temperature amplifies with an upsurging heat source/sink parameter. Recently, Ghasemi and Hatami [13] scrutinized the consequence of incorporating thermal radiation on the stagnation point fluid flow across a stretching sheet. "It is often argued that heat transfer, mass deposition, pressure, and other parameters are at their highest rates near the stagnation point." [14]

"All the above investigations are, however, confined to flows of Newtonian fluids. In recent years, it has generally been recognized that in industrial applications, non-Newtonian fluids are more appropriate than Newtonian fluids. For instance, in certain polymer processing applications, one deals with the flow of a non-Newtonian fluid over a moving surface. That non-Newtonian fluids are finding increasing application in industry has given impetus to many researchers." Casson fluid is the most crucial type among various non-Newtonian fluids [15]. "Examples of Casson fluid include jelly, tomato sauce, honey, soup, and concentrated fruit juices, etc. Human blood can also be treated as Casson fluid." Leveraging the Homotopy Analysis Method, Mustafa et al. [16] procured the solution of Casson fluid flow adjacent to the stagnation point across stretching surfaces analytically. They furnished the outcomes pertaining to a unique situation where the Casson parameter goes to infinity. In fluid mechanics, as the name suggests, viscous dissipation occurs by virtue of viscous stresses and is the eradication of fluctuating velocity gradients. This partially irreversible process transforms the fluid's kinetic energy into internal energy. It was concluded by Mustafa et al. [16] that the Eckert number (viscous dissipation parameter) augments the temperature. Bhattacharyya [17] inquired about heat transfer at the stagnation point of Casson fluid flow past a shrinking/stretching sheet. He employed the classical Runge-Kutta RK4 shooting technique, out of which he stated that "the range of velocity

ratio parameter for which similarity solution exists is unaltered for any change in Casson parameter." Exact solutions were procured for the heat transfer effects across a stretching sheet by Mukhopadhyay et al. [18] and Bhattacharyya et al. [19]. Ultimately, they inferred that the impact of rising values of the Casson parameter depletes the velocity, but on the contrary, the temperature is augmented. Bhattacharyya [20] "considered two-dimensional magnetohydrodynamic stagnation point flow of an electrically conducting Casson fluid and heat transfer due to a stretching sheet under the effect of thermal radiation." It was alluded by them that the fluid's velocity depreciates with augmenting velocity ratio parameter. Kameswaran et al. [21] emphasized the significance of stagnation point flow on the simultaneous heat and mass transfer problem beyond a shrinking/stretching sheet. He employed the MATLAB bvp4c ODE solver for a Casson fluid flow and declared that an escalation in the stretching ratio upsurges the fluid velocity, which consequently diminishes the concentration. Of late, Lund et al. [22] reinspected the impact of viscous dissipation and radiation of stagnation point Casson fluid flow towards shrinking/stretching surfaces. Observations made by them stated that the temperature skyrocketed with an escalating Eckert number and radiation.

All the aforementioned studies were accomplished by taking into consideration that the fluid exhibits constant physical properties, but pragmatic circumstances necessitate variable physical properties [23]. "Thermal conductivity is one of such properties, which is assumed to vary linearly with the temperature. The variation in conductivity considered as a function of temperature is seen to be approximately linear as shown in Kays and Crawford [24], in the range of temperatures 0°F to 400°F." [25] A "semi-empirical formula" of the aforementioned form for the thermal conductivity was extrapolated and solved using the regular perturbation technique by Arunachalam and Rajappa [26]. Chiam [27] obtained both closed-form analytical solutions and numerical solutions of stagnation point flow accompanied by variable thermal conductivity past a stretching sheet. A similar work to [27] was carried out by Chiam [28], in which he analysed the influence of variable thermal conductivity on flow along a linearly stretching sheet. Unlike [27], in [28], it was concluded that a copious amount of computational work was minimized by the employment of the Runge Kutta algorithm-based shooting technique. Over a decade later, Sharma and Singh [29] inspected the consequences of variable thermal conductivity by incorporating a magnetic field in the vicinity of a stagnation point across a linearly stretching sheet. He exploited a fourth-order Runge-Kutta-based shooting scheme and reported that the Hartmann number tends to proliferate with temperature. The above-mentioned studies on variable thermal conductivity did not focus on non-Newtonian fluids. This motivated Venkateswarlu and Satya Narayana [30] to assess the effect of Casson fluid flow with variable thermal conductivity and viscous dissipation over a stretching sheet under the existence of mass transfer. Numerical computations were carried out by them, and they stated that the temperature enhances with augmenting Eckert number and Casson fluid parameter. Modern research by Yu et al. [31] showed that it is necessary for the lunar lander to dissipate heat during the lunar day for the purpose of maintaining the instrument module warm during the lunar night. This could only be accomplished by variable thermal conductivity. This essentiality of variable thermal conductivity in the technology of lunar soft landers serves as evidence for its indispensability in the field of the aerospace industry. In the recent past, Dhange et al. [32] inspected variable thermal conductivity effects on MHD Casson fluid flow across a stretching sheet.

Due to the overwhelming practical applications of heat source/sink, it is noteworthy to consider their impact on heat transfer processes [33, 34]. Though heat source/sink have a uniform rate within the conducting medium [35], in many situations of practical importance, it is often argued that the temperature-dependent and space-dependent modes are the two acceptable modes of heat source and heat sink. Even though its influence may be regarded as constant, some scientists claim it to be varying or non-uniform. Initial studies by Abo-Eldahab and El Aziz [36] were carried out on the impact of non-uniform heat source, but were constrained to Newtonian fluids. Under the impingement of internal heat absorption/generation, it was declared by them that an upsurge in magnetic parameter decreased the Nusselt number and friction factor. Motivated by the preceding article under discussion, Abel and Mahesha [37] explored the viscoelastic fluid flow past stretching surfaces by incorporating a non-uniform heat sink/source (internal heat absorption/generation) together with variable thermal conductivity. Additionally, it was concluded by them that "the effect of space and temperature dependent heat source/sink parameters is to generate temperature for increasing positive values and absorbs temperature for decreasing negative values." Moreover, under the prescribed surface temperature, the variable thermal conductivity parameter resulted in an upsurge in temperature. We will, however, not repeat this analysis here. Nevertheless, this investigation by Abel and Mahesha [37] stands as evidence for the combined existence of variable thermal conductivity together with a non-uniform heat sink/source in the fluid flow. Later, Monica and Sucharitha [38] scrutinized the non-uniform heat source/sink for different fluids and under different geometry. It was inferred by them that, upon the existence of internal heat absorption/generation, escalating values of the Casson fluid parameter amplified the temperature. A recent numerical analysis was undertaken by Li et al. [39] on the Casson nanoparticles in the vicinity of the stagnation point, together with internal heat absorption/generation and viscous dissipation. It is obvious that the results obtained from the shooting technique graphically represent that the velocity diminishes as the Casson fluid parameter shoots up.

"Convective heat transfer studies are very important in processes involving high temperatures, such as gas turbines, nuclear plants, and thermal energy storage." Pioneering work on the interaction between radiation and natural convection was carried out by Ali et al. [40]. The hot and cold surfaces were considered, and dimensionless temperatures for both were explicitly mentioned. It was Aziz [41] who initiated the inspection of the convective surface boundary condition. A noteworthy equation of boundary conditions far away from the fluid and on the surface was mentioned. By extending the work of [41], Ishak [42] obtained similarity solutions for heat transfer in the fluid flow by incorporating convective boundary conditions. The impact of convective boundary conditions over a stretching surface was scrutinized by Makinde and Aziz [43]. It was concluded numerically by them that the rising values of the Biot number, which characterize convective heating, tend to enhance the temperature distribution. With the incorporation of the convective boundary condition, Yao et al. [44] inspected the problem of heat transfer and obtained the exact solution. The numerical solution for stagnation-point flow with convective boundary conditions across a stretching sheet was discussed by Mohamed et al. [45]. The shooting technique was employed, and an enhancement in the stretching parameter increased the velocity profile. All the aforesaid surveys on convective boundary conditions did not take Casson fluid into consideration. Recently, Raza [46] scrutinized the flow of a chemically reacting Casson fluid at a stagnation point past a convective stretching sheet. He employed the Runge-Kutta Fehlberg scheme to conclude that the rising Schmidt number diminishes the concentration. Dessie [47] extended the work of [46] by employing the Lie-group analysis technique and the Runge-Kutta method on stagnation-point Casson fluid flow to study the consequences of viscous dissipation, thermal radiation, and partial slip over a convective stretching sheet. It is obvious that the fluid's velocity declines as velocity slip skyrockets. Moreover, the intensification of homogenous chemical reactions diminishes the concentration of the flow.

Convective flows, along with the impact of chemical reactions and accompanied by simultaneous heat and mass transfer, emerge in various transport processes. This occurs in diverse fields of science and engineering applications, both naturally and artificially. Moreover, this phenomenon plays a crucial role in chemical vapor deposition on surfaces, power and cooling industries, hydrometallurgical industries [48], and petroleum industries [49]. "Irreversible chemical reaction and differences in the molecular weight between the values of the reactants and the products" cause changes in fluid density gradients. Chemical reactions are classified as either homogenous or heterogeneous. This is determined by "whether it is a single-phase volume reaction or the reaction occurs at an interface." At a given phase, a reaction that occurs uniformly throughout is said to be a homogeneous reaction. A heterogeneous reaction, on the other hand, occurs within a phase's boundary or in a restricted area. Pioneering work on constructive or destructive chemical reactions from a stretching sheet was undertaken by Andersson et al. [50]. Vajravelu et al. [51] employed the Keller-box scheme to numerically study the "diffusion of a chemically reactive species from a stretching surface." The consequences of destructive/constructive chemical reactions on viscous incompressible fluids were assessed by Bhattacharyya et al. [52] and emphasized the fact that chemical reactions are vital in the diffusion of concentration. With the employment of the Runge-Kutta method, they stated that the concentration decreased with augmenting the reaction rate. "Diffusion of chemically reactive species in Casson fluid flow" past stretching surfaces was shed light on by Mukhopadhyay and Vajravelu [53]. Abbas et al. [54] analyzed the "diffusion of chemically reactive species in stagnation-point flow." With different geometry under consideration, the constructive and destructive chemical rates with a uniform heat sink/source were scrutinized by Jena et al. [55]. Recently, Khan et al. [56] inspected the consequences of constructive/destructive chemical reactions in viscous fluids with the existence of convective boundary conditions via the Homotopy Analysis Method. A detailed review of convective boundary layer flow problems on various mathematical models was presented by Kanafiah et al. [57].

Keeping the above-mentioned things in mind and to the best of the authors' knowledge, no prior study was accomplished to inspect the combined impact of a non-uniform heat source/sink (internal heat generation/absorption) and variable thermal conductivity on the stagnation point flow of Casson fluid. Inspired by the afore-mentioned surveys, the present article probes to inspect the influence of stagnation point flow on Casson fluid with internal heat generation/absorption and variable thermal conductivity past a convective stretching sheet under the influence of constructive/destructive chemical reactions. This stands as the prime novelty behind this study. Respective ordinary differential equations (ODEs) that correspond to the governing PDEs are acquired by virtue of an ideal similarity transformation. Then the resulting equations are cracked by employing bvp4c, an in-built MATLAB technique. Graphical solutions are depicted for the impact of pertinent parameters on velocity profiles, temperature distributions, and concentration distributions. Also, values of the skin friction coefficient, Nusselt number, and Sherwood number are presented in tabular form. In a constrained scenario, the solutions obtained are validated against the pre-existing literature. The essentiality of variable thermal conductivity in the lunar soft lander technology serves as evidence for its indispensability in the field of aerospace industry.

MATHEMATICAL FORMULATION

Consider a steady electrically conducting viscous incompressible Casson fluid past a stretching sheet. The x-axis is assumed to be along the stretched sheet. Additionally, the

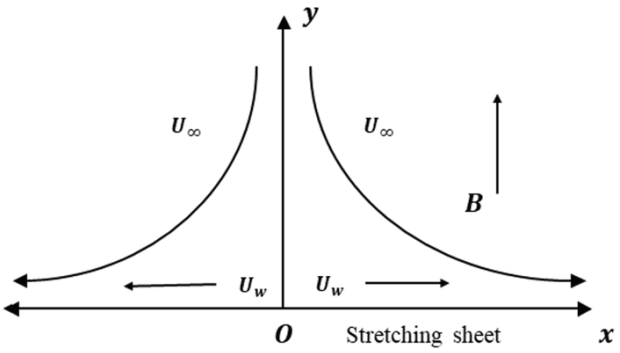

Figure 1. Schematic diagram of the flow problem.

y-axis is presumed to be normal to the *x*-axis. The stagnation point is at the origin *O*. Two equal and opposite forces are applied along the *x*–axis by retaining fixed origin, which causes the sheet to stretch with a velocity $U_w(x) = cx$ (for $c > 0$). It is presumed that the flow is constrained to the half plane $y > 0$. Moreover, a uniform magnetic field of strength *B* is imposed in the transverse direction. It is anticipated that the sheet's surface is heated convectively from a hot fluid that possesses heat exchange coefficient h_f and temperature T_f. In the same way, the Casson fluid's free stream velocity is acknowledged as $U_\infty(x) = ax$ (for $a > 0$). Furthermore, it is postulated that, at the fluid interface, there exists a partial velocity slip [47] (Fig. 1).

The rheological equation of state for an isotropic and incompressible flow of a Casson fluid is

$$\tau_{ij} = \begin{cases} 2\left(\mu_B + \dfrac{p_y}{\sqrt{2\pi}}\right)e_{ij}, & \pi > \pi_c \\ 2\left(\mu_B + \dfrac{p_y}{\sqrt{2\pi_c}}\right)e_{ij}, & \pi < \pi_c \end{cases} \tag{1}$$

where e_{ij} is the $(i,j)^{th}$ component of the deformation rate, π is the product of the component of deformation rate with itself, $\pi = e_{ij}e_{ij}$, π_c is the critical value of this product based on the non-Newtonian model, μ_B is the plastic dynamic viscosity of the non-Newtonian fluid, and p_y is the yield stress of the fluid." [18]

Regarding Casson fluid, where $\pi > \pi_c$ and $p_y = \frac{\mu_B\sqrt{2\pi}}{\beta}$, the dynamic viscosity is

$$\mu = \mu_B + \frac{p_y}{\sqrt{2\pi}} \tag{2}$$

Upon substitution of p_y in (2), we get

$$\mu = \mu_B\left(1 + \frac{1}{\beta}\right) \tag{3}$$

where β known as the Casson fluid parameter, quantifies the non-Newtonian behavior, impacting the fluid's viscosity and yield stress. The flow becomes Newtonian as $\beta \to \infty$.

Corresponding to the framework under deliberation, the governing equations are formulated as: [47]

$$\frac{\partial u}{\partial x} + \frac{\partial v}{\partial y} = 0 \tag{4}$$

$$u\frac{\partial u}{\partial x} + v\frac{\partial v}{\partial y} = U_\infty\frac{dU_\infty}{dx} + \nu\left(1 + \frac{1}{\beta}\right)\frac{\partial^2 u}{\partial y^2} + \frac{\sigma B^2}{\rho}(U_\infty - u) \tag{5}$$

$$\rho c_p\left(u\frac{\partial T}{\partial x} + v\frac{\partial T}{\partial y}\right) = \frac{\partial}{\partial y}\left(K\frac{\partial T}{\partial y}\right) - \frac{\partial q_r}{\partial y} + q''' + \mu_B\left(1 + \frac{1}{\beta}\right)\left(\frac{\partial u}{\partial y}\right)^2 + \sigma B^2(U_\infty - u)^2 \tag{6}$$

$$u\frac{\partial C}{\partial x} + v\frac{\partial C}{\partial y} = D\frac{\partial^2 C}{\partial y^2} - k_1(C - C_\infty) \tag{7}$$

Here, *K* is the variable thermal conductivity. q''' is the non-uniform heat source/sink. q_r is the radiative heat flux. *D* is the coefficient of mass diffusivity. Moreover, k_1 is the reaction rate, where $k_1 > 0$ signifies destructive reaction and $k_1 < 0$ corresponds to constructive reaction. Utilizing Rosseland approximation [58] for thermal radiation, q_r is expressed as:

$$q_r = -\frac{4\sigma^*}{3k^*}\frac{\partial T^4}{\partial y}, \tag{8}$$

where k^* is the "absorption coefficient" and σ^* is the "Stefan–Boltzmann constant". "We assume that the temperature differences within the flow are such that T^4 may be expressed as a linear function of temperature. This is accomplished by expanding T^4 in a Taylor series about T_∞ and neglecting higher order terms, thus" [4]

$$T^4 \equiv 4T_\infty^3 T - 3T_\infty^4 .$$

With reference to Chiam [34], *K* is expressed as:

$$K = K_\infty(1 + \varepsilon\theta), \tag{9}$$

where $\theta = \frac{T - T_\infty}{T_f - T_\infty}$ and $\varepsilon = \frac{K_W - K_\infty}{K_\infty}$ (ε - small parameter).

Moreover, q''' is modelled with the following equation as reference:

$$q''' = \frac{KU_w}{xv}\left[A^*(T_f - T_\infty)f' + B^*(T - T_\infty)\right], \tag{10}$$

where A^* is the "coefficient of space-dependent internal heat generation/absorption" and B^* is "coefficient of temperature-dependent internal heat generation/absorption". When both $A^* > 0$ and $B^* > 0$ this denotes "internal heat

generation" and when both $A^* < 0$ and $B^* < 0$ this indicates "internal heat absorption." [36]

The pertinent boundary conditions [47] are:

$$\text{at } y = 0 : u = U_w + L\frac{du}{\partial y} = cx + L\frac{du}{\partial y}, v = 0, \\ -K\frac{\partial T}{\partial y} = h_f\left(T_f - T\right) \text{ and } C = C_w. \quad (11)$$

$$\text{as } y \to \infty : u \to U_\infty = ax, T \to T_\infty \text{ and } C \to C_\infty. \quad (12)$$

Solution Technique

In order to procure the corresponding ODEs pertaining to the PDEs that govern the fluid flow, a suitable similarity transformation is employed. As mentioned by Aziz [41] and Raza [46], a suitable similarity transformation with η as the similarity variable is introduced as follows:

$$\eta = y\sqrt{\frac{a}{\nu}} \quad (13)$$

$$\psi(x, y) = \sqrt{av}\, x\, f(\eta) \quad (14)$$

$$\theta(\eta) = \frac{T - T_\infty}{T_f - T_\infty} \quad (15)$$

$$\phi(\eta) = \frac{C - C_\infty}{C_w - C_\infty} \quad (16)$$

Upon substitution of equations (8) – (10) and (13) – (16) in equations (4) – (7), (11) and (12), we get the transformed governing equations as

$$\left(1 + \frac{1}{\beta}\right) f''' + ff'' - f'^2 + M(1 - f') + 1 = 0 \quad (17)$$

$$(1 + \varepsilon\theta + N)\theta'' + \varepsilon\theta'^2 + \alpha(1 + \varepsilon\theta)(A^* f' + B^*\theta) \\ + Ec\, Pr\left(1 + \frac{1}{\beta}\right) f''^2 + \Pr f\theta' + M\, Ec \Pr(1 - f')^2 = 0 \quad (18)$$

$$\phi'' + Sc\, f\phi' - k\, Sc\, \phi = 0 \quad (19)$$

together with the transformed boundary conditions as follows:

$$\text{at } \eta = 0: f' = \alpha + Af'', f = 0, \theta' = -Bi\left(\frac{1 - \theta}{1 + \varepsilon\theta}\right) \text{ and } \phi = 1. \quad (20)$$

$$\text{as } \eta \to \infty : f' \to 1, \theta \to 0 \text{ and } \phi \to 0. \quad (21)$$

Various dimensionless parameters obtained during this transformation are

$$M = \frac{\sigma B^2}{\rho a}, N = \frac{16\sigma^* T_\infty^3}{3k^* K_\infty}, \alpha = \frac{c}{a}, Ec = \frac{U_\infty^2}{c_p(T_f - T_\infty)}, \\ Pr = \frac{\mu c_p}{K_\infty}, Sc = \frac{\nu}{D}, k = \frac{k_1}{a}, A = L\sqrt{\frac{a}{\nu}} \text{ and} \\ Bi = -\frac{h_f}{K_\infty}\sqrt{\frac{\nu}{a}}.$$

The quantities which are of physical importance (namely C_{fx}, Nu_x and Sh_x) are acquired as follows:

$$C_f = C_{f_x}\sqrt{Re_x} = \left(1 + \frac{1}{\beta}\right) f''(0) \\ Nu = \frac{Nu_x}{\sqrt{Re_x}} = -\theta'(0) \\ Sh = \frac{Sh_x}{\sqrt{Re_x}} = -\phi'(0),$$

where $Re_x = \frac{xU_\infty}{\nu}$ is the local Reynolds number, $\frac{Sh_x}{\sqrt{Re_x}}$ is the reduced Sherwood number Sh, $\frac{Nu_x}{\sqrt{Re_x}}$ is the reduced Nusselt number Nu, and $C_{fx}\sqrt{Re_x}$ is the reduced skin friction coefficient C_f.

Numerical Procedure

"It is not always easy to solve the equations analytically; thus one may need numerical methods in that scenario". Various numerical methods employed to solve the heat and mass transfer problem of Casson fluids were presented as a brief review in [59]. The boundary value problems (BVPs) are resolved numerically by means of MATLAB. The transmogrified governing equations (17)-(19) accompanied by the transmogrified boundary conditions (20) and (21) are numerically resolved by implementing the bvp4c package of MATLAB. "bvp4c is a finite difference algorithm that incorporates the three-stage Lobatto IIIa collocation formula. bvp4c can be effectuated by altering the BVP as an initial value problem (IVP)" [60]. In MATLAB, when solving BVPs the user must provide a guess to assist the solver in computing the desired solution. MATLAB BVP solvers call for users to provide guesses for the mesh and solution. Although MATLAB BVP solvers take an unusual approach to the control of error in case of having poor guesses for the mesh and solution, especially for the nonlinear BVP, a good guess is necessary to obtain convergence. The calculations are simulated using the MATLAB R2019a on a laptop with Intel Core i5 2.40 GHz. Moreover, this method delivers enhanced computing results with minimal CPU time (~1–2 seconds) per evaluation. The following linearity technique is deployed:

"$y_1 = f, y_2 = f', y_3 = f'', y_4 = \theta, y_5 = \theta', y_6 = \varphi$ and $y_7 = \varphi'$," and hence the equations (17)-(19) become

$$y_3' = \frac{1}{\left(1 + \frac{1}{\beta}\right)}[y_2 y_2 - y_1 y_3 - M(1 - y_2) - 1],$$

$$y_5' = \frac{1}{(1+\varepsilon y_4+N)}\Big[-\varepsilon y_5 y_5 - \alpha(1+\varepsilon y_4)(A^* y_2 + B^* y_4) - Ec\,\mathrm{Pr}\left(1+\frac{1}{\beta}\right) y_3 y_3 - \mathrm{Pr}\, y_1 y_5 - M\, Ec\,\mathrm{Pr}(1-y_2)^2\Big]$$

and y_7' = -$Sc\, y_1\, y_7 + kScy_6$

Moreover, the boundary conditions are articulated as:

$y_2(0) = \alpha + Ay_3(0)$, $y_1(0) = 0$, $y_5(0) = -Bi\left(\frac{1-y_4(0)}{1+\varepsilon y_4(0)}\right)$, $y_6(0) = 1$, $y_2(\infty) \to 1$, $y_4(\infty) \to 0$ and $y_6(\infty) \to 0$.

However, the outcomes are evaluated at the far field $\eta_\infty = \eta_{max}$ (= 5).

RESULTS AND DISCUSSION

Validation of the Numerical Outcomes

To corroborate the authenticity of the numerical technique employed, the values of $f''(0)$, $-\theta'(0)$ and $-\phi'(0)$ under a constrained scenario are correlated with the pre-existing outcomes that are available in the literature. For Newtonian fluid in the absence of a magnetic field, the values of $f''(0)$ for numerous α was deduced and tabulated in Table 1. The outcomes procured match those of [8] and [17]. The outputs of heat transfer coefficient $-\theta'(0)$ for various α under limiting cases are compared with those of [8] and [21] (Table 2). The numerical values obtained exhibit a good agreement. Moreover, it is perceivable that α amplifies the heat transfer. For specific chemical reaction parameter, Schmidt number, and for a Casson fluid, the values of $-\phi'(0)$ are obtained and tabulated (Table 3). Under special case, the values are in best accord with those of [46] and [47].

Impact of Several Parameters on C_f, *Nu* and *Sh*

The values of C_f, *Nu* and *Sh* for multifarious pertinent parameters are tabulated in Tables 4, 5 and 6 respectively. C_f reduces with a rise in M and α. However, the reverse phenomenon is observed for A and β. These are obviously depicted in Table 4. From the Table 5, it is manifested that an enhancement in α and Bi skyrockets the heat transfer.

Table 1. Comparison of $f''(0)$ with Wang [8] and Bhattacharyya [17] for several values of velocity ratio parameter

α	$f''(0)$		
	Wang [8]	**Bhattacharyya [17]**	**Present Study**
0	1.232588	1.2325878	1.232587589
0.1	1.14656	1.1465608	1.146560931
0.2	1.05113	1.0511299	1.051129925
0.5	0.71330	0.7132951	0.713294910
1	0	0	0

Table 2. Comparison of $-\theta'(0)$ with Wang [8] and Kameswaran et al. [21] for several values of velocity ratio parameter

α	$-\theta'(0)$		
	Wang [8]	**Kameswaran et al. [21]**	**Present Study**
0	0.811301	0.8113013	0.811301532
0.1	0.86345	0.8634517	0.863451813
0.2	0.91330	0.9133028	0.913302946
0.5	1.05239	1.0514584	1.051458489
1	1.25331	1.2533141	1.253314154

Table 3. Comparison of $-\phi'(0)$ with Raza [46] and Dessie [47] for several values of Sc and k when Pr = 0.7, M = 0.5, A = 0.5, β = 0.3 and Bi = 0.2

Sc	k	$-\phi'(0)$		
		Raza [46]	**Dessie [47]**	**Present study**
0.5	0.5	0.60627	0.6062704	0.6062745
1.0	0.5	0.80891	0.8089132	0.8089160
1.5	0.5	0.93656	0.9365614	0.9365605
2.0	0.5	1.02588	1.0259312	1.0259353
0.7	0	0.91982	0.9198254	0.9198258
0.7	0.5	0.70096	0.7009613	0.7009618
0.7	1.0	0.50891	0.5089122	0.5089134
0.7	2.0	0.22047	0.2204713	0.2204715

But, on the contrary, *Nu* declines with increasing values of M, ε, N, Ec, A^*, B^*, A and β. Also, *Sh* reduces with increasing M, A and β but, skyrockets with enhancement of α and k (Table 6). Under limiting cases, the results match those of [46] and [47].

Table 4. Numerical values of C_f for fixed values Pr = 0.7, Sc = 0.7, ε = 0.2, N = 1, Ec = 0.01, $A^\star = B^\star$ = -0.01, k = 0.3 and Bi = 0.5

M	α	A	β	$\left(1+\frac{1}{\beta}\right)f''(0)$
0.5	2	2.5	0.2	-1.56663
2.5				-1.68475
5.5				-1.79015
0.5	2.5			-2.36958
	3			-3.18355
	2	4		-1.12166
		7.5		-0.67643
		2.5	0.8	-0.67635
			2.5	-0.44357

Table 5. Numerical values of *Nu* for fixed values *Pr* = *Sc* = 0.7

M	*ε*	*N*	*Ec*	*A**	*B**	*α*	*A*	*Bi*	*β*	-*θ*′(0)
0.5	0.2	1	0.01	–0.01	–0.01	2	2.5	0.5	0.2	0.25790
2.5										0.25534
5.5										0.25321
0.5	0.5									0.23963
	1.2									0.20923
	0.2	3								0.21214
		5								0.18662
		1	0.05							0.25616
			0.1							0.25400
			0.01	0.01						0.22345
				0.02						0.20617
				–0.01	0.02					0.25282
					0.04					0.24920
					–0.01	2.5				0.26711
						3				0.27575
						2	4			0.25508
							7.5			0.25197
							2.5	0.8		0.31717
								1.2		0.36445
								0.5	0.8	0.25316
									2.5	0.25141

Table 6. Numerical values of Sh for *Pr* = 0.7, *Sc* = 0.7, *ε* = 0.2, *N* = 1, *Ec* = 0.01, *A** = *B** = -0.01 and *Bi* = 0.5

M	*α*	*A*	*β*	*k*	-*ϕ*′(0)
0.5	2	2.5	0.2	0.3	0.86187
2.5					0.84897
5.5					0.83788
0.5	2.5				0.89139
	3				0.91935
	2	4			0.84456
		7.5			0.82645
		2.5	0.8		0.83580
			2.5		0.82602
			0.2	0.5	0.93495
				1	1.09948

Impact of Involved Parameters on Velocity Profile *f*′(*η*), Temperature Distribution *θ*(*η*) and Concentration Distribution *ϕ*(*η*)

To elucidate briefly, the striking effect of various pertinent parameters on $f'(\eta)$, $\theta(\eta)$ and $\phi(\eta)$ are demonstrated through figures. The values $\beta = 0.2$, $M = 0.5$, $\varepsilon = 0.2$, $N = 1$, $\alpha = 2$, $A^* = B^* = -0.01$, $Ec = 0.01$, $Pr = 0.7$, $Sc = 0.7$, $k = 0.3$, $A = 0.5$ and $Bi = 0.5$ are taken as fixed throughout this numerical study, except the varying values are clearly noted in the respective figures.

Figure 2 demonstrates the consequence of magnetic field parameter M on $f'(\eta)$. The transport rate declines by virtue of transverse magnetic field. This is due to the drag which gets developed due to Lorentz force. The existence of magnetic field in an electrically conducting fluid tends to produce a dragging or retarding force against the flow. "This type of resistive force tends to slow down the motion

of the fluid in the boundary layer which, in turn, reduces the rate of heat convection in the flow and this appears in increasing the flow temperature." A strong Lorentz force acts as a medium to generate more heat to the fluid from the surface. Hence, the temperature distribution $\theta(\eta)$ gets enhanced as M rises which is evident from Figure 3.

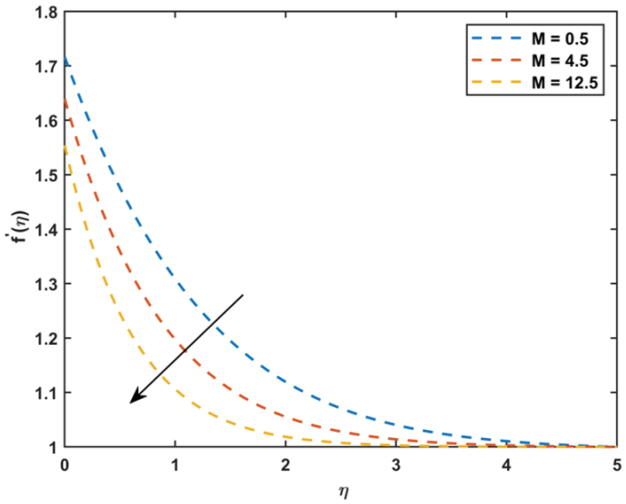

Figure 2. Velocity profile for various M.

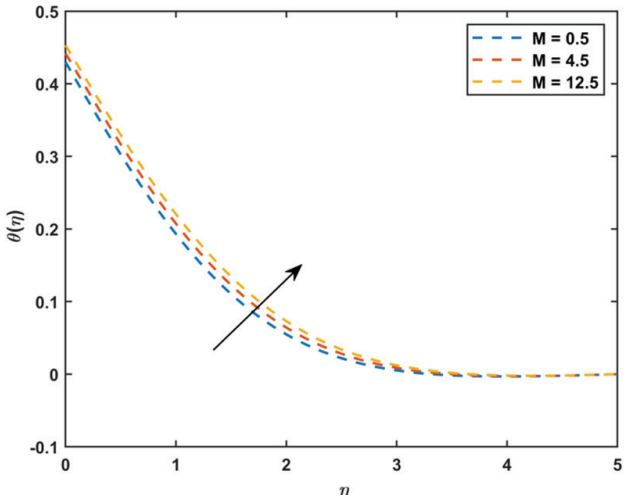

Figure 3. Temperature distribution for various M.

It is perceptible from Figure 4 that the enhancement of the Casson parameter β declines $f'(\eta)$. This is attributable to the fact that an upsurge in β diminishes the yield stress, which results in a reduction of the velocity. Higher values of β creates a resistance to the fluid flow. Physically, flows with high Casson number corresponds to solid-like behaviour. Moreover, it is noteworthy to mention that as $\beta \to \infty$, the fluid behaves like a Newtonian fluid i.e., simple viscous fluid. Quite opposite behaviour is perceived for augmenting values of β on the temperature distribution (Fig. 5). This reduction in $\theta(\eta)$ is by virtue of rising Casson parameter which is related to declination of the fluid's yield stress.

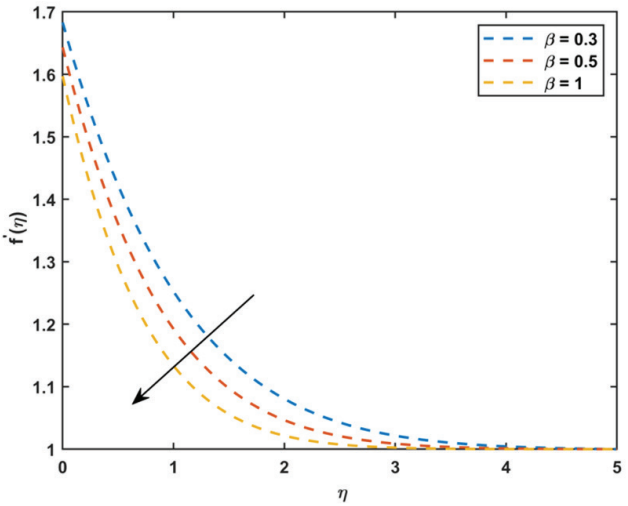

Figure 4. Velocity profile for various β.

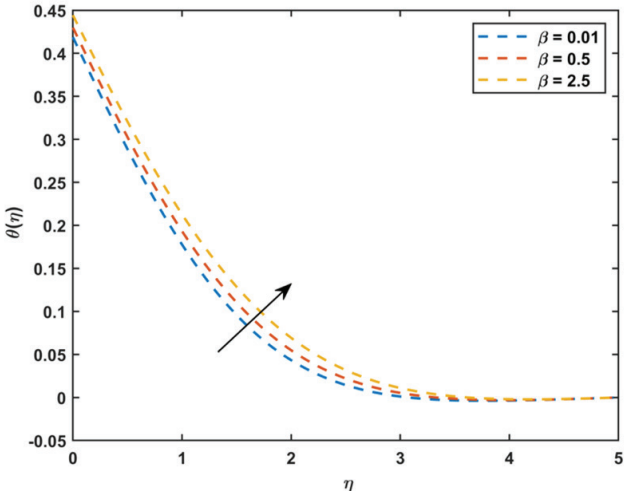

Figure 5. Temperature distribution for various β.

The consequence of variable thermal conductivity parameter ε on the temperature distribution is demonstrated in Figure 6. The variation range of ε is regarded as, "for air $0 \le \varepsilon \le 6$, for water $0 \le \varepsilon \le 0.12$ and for lubrication oils $-0.1 \le \varepsilon \le 0$" [61]. Simultaneous effect of non-uniform heat source/sink and variable thermal conductivity plays a major role in the temperature distribution of the convective stretching sheet under consideration. As both $A^* > 0$ and $B^* > 0$ i.e., for internal heat generation, an increase in ε reduces the temperature. But this is not the case for internal heat absorption. i.e., both $A^* < 0$ and $B^* < 0$, an enhancement in ε, diminishes $\theta(\eta)$ very near to the wall and as the fluid

moves away from the wall, $\theta(\eta)$ skyrockets. This dramatic effect is due to the influence of variable thermal conductivity in the convective boundary condition.

The impact of incorporating the thermal radiation in the energy equation is delineated in Figure 7. Escalation of the temperature domain in the fluid flow is observed when thermal radiation is taken into consideration. This is by virtue of the enhancement of K_∞ in an electrically conducting fluid. In addition, physically, this is in consonance with the aspect that amplifying N augments the thermal boundary layer thickness. Intensification of the effective thermal diffusivity occurs due to thermal radiation which results in proliferation of $\theta(\eta)$. This shows that the radiation parameter positively impacts the convective heat transfer.

The effect on velocity ratio parameter (α) on $f'(\eta)$, $\theta(\eta)$ and $\phi(\eta)$ are illustrated in Figures 8 – 10 respectively. When $\alpha > 1$, it implies that the free stream velocity is lesser than the surface velocity. In such a situation, the flow velocity $f'(\eta)$ skyrockets as α rises. When $\alpha = 1$, it corresponds to the case when stretching velocity and free stream velocity are equal. It is conspicuous from the figure that when the free stream and stretching velocities are equal, "there is no boundary layer of Casson fluid flow" in close proximity to the surface. It is observed that for $\alpha < 1$, i.e., the free stream velocity outstrips the surface velocity, the fluid flow's velocity augments with an increase in α. There is a decline in $\theta(\eta)$ and $\phi(\eta)$ for rising values of several α. This is obvious from Figures 9 and 10 respectively.

"The Eckert number provides a measure of the kinetic energy of the flow relative to the enthalpy difference across the thermal boundary layer. It is used to characterize heat dissipation in high-speed flows for which viscous

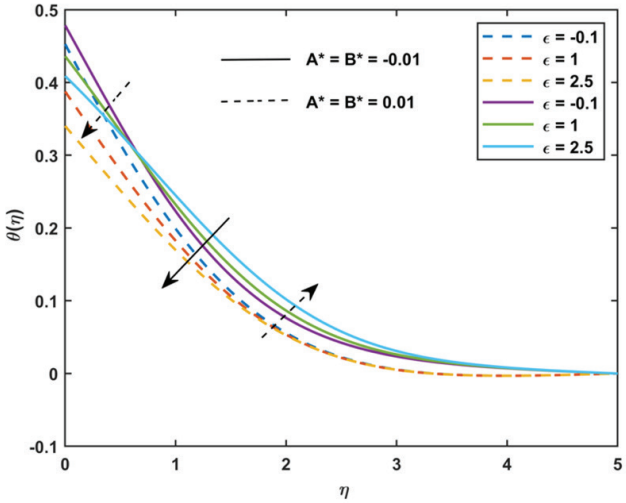

Figure 6. Temperature distribution for various ε.

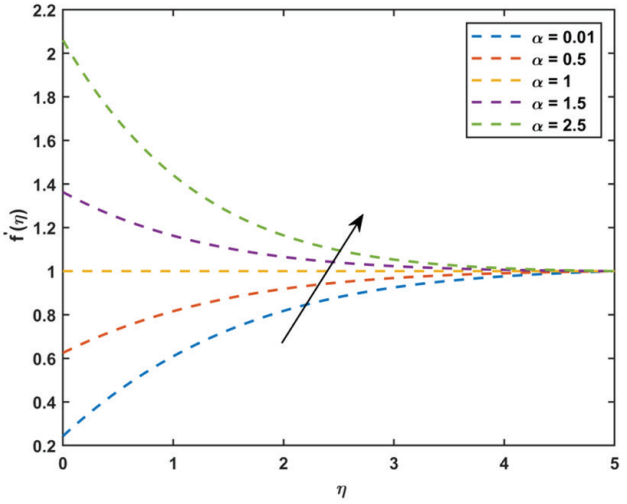

Figure 8. Velocity profile for various α.

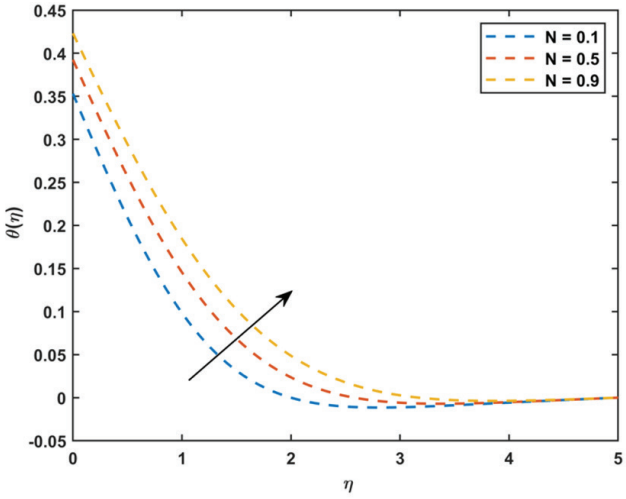

Figure 7. Temperature distribution for various N.

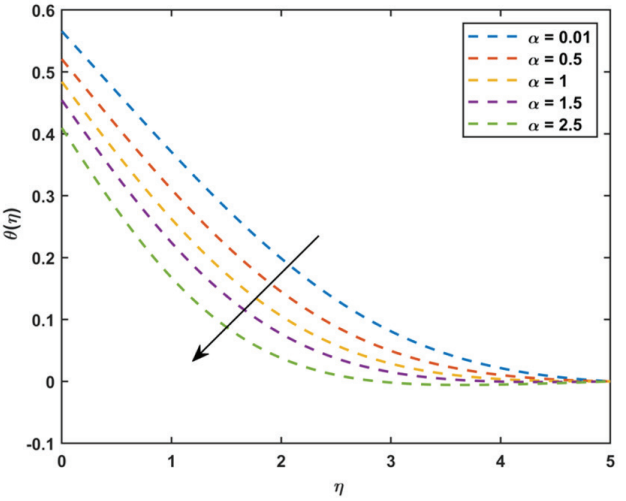

Figure 9. Temperature distribution for various α.

dissipation is significant." From Figure 11, "it is evident that $\theta(\eta)$ skyrockets as Ec augments. This occurs due to frictional heating in the fluid which causes heat to be generated as Ec increases. Consequently, an upsurge in Ec leads to work being done against the stresses of the viscous fluid, which transmutes kinetic energy into internal energy. Also, Eckert number signifies the quantity of mechanical energy converted via internal friction to thermal energy i.e., heat dissipation. This indirectly emphasizes the vitality of viscous dissipation in the energy equation.

Figure 12 portrays the consequence of space-dependent internal heat generation/absorption parameter A^* on $\theta(\eta)$. The graph demonstrates that the energy gets released for rising $A^* > 0$ (heat source) whereas the energy gets absorbed for $A^* < 0$ (heat sink) for decreasing A^* which in turn causes $\theta(\eta)$ to fall considerably. Similarly, the striking consequence of temperature-dependent internal heat generation/absorption parameter B^* is illustrated in Figure 13. Particularly, when $B^* < 0$ (heat sink), the energy gets absorbed in the boundary layer for decreasing B^* which eventually reduces $\theta(\eta)$. But, for augmenting values of $B^* > 0$ (heat source), the energy gets generated which cause the temperature to augment.

The simultaneous effect of Pr and Sc on $\theta(\eta)$ and $\phi(\eta)$ are scrutinized in Figures 14 and 15 respectively. The impacts are evaluated for air (Pr = 0.7, Sc = 0.7), methanol at 25°C (Pr = 6.83, Sc = 1.14) and ethanol at 25°C (Pr = 18.05, Sc = 1.29). Simultaneous rise of Schmidt number and Prandtl number reduces the temperature adjacent to the wall but contrarily, enhances away from the wall. When both Schmidt number and Prandtl number rises, a reduction in concentration distribution is observed. These

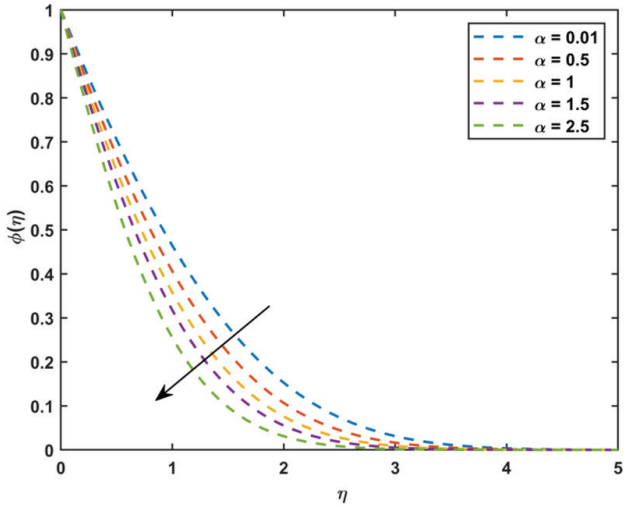

Figure 10. Concentration distribution for various α.

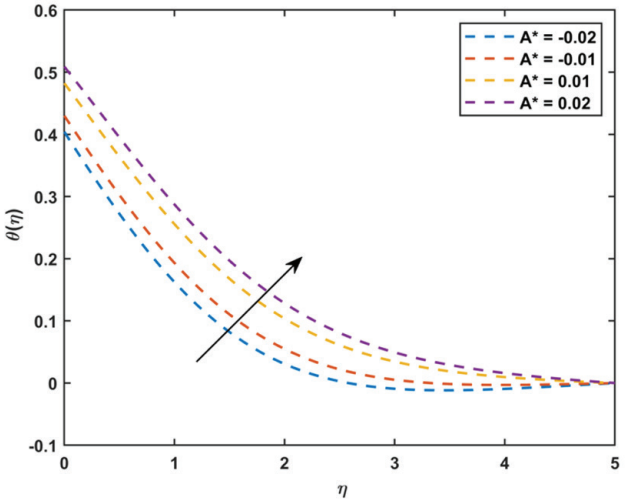

Figure 12. Temperature distribution for various A^*.

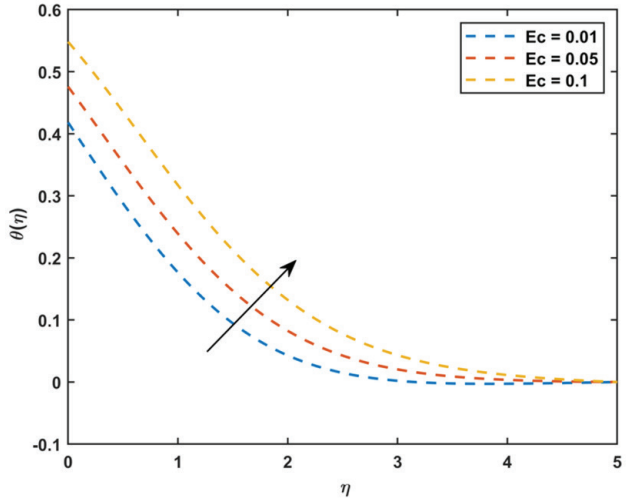

Figure 11. Temperature distribution for various Ec.

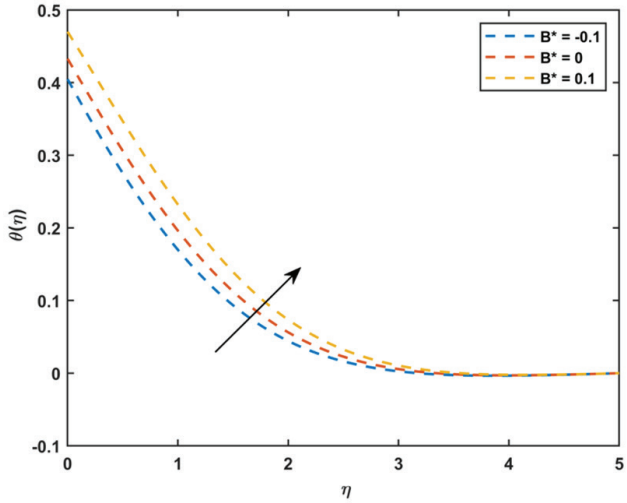

Figure 13. Temperature distribution for various B^*.

results are attributable to the fact that the Prandtl number has a negative relationship with thermal conductivity and Schmidt number has a negative relationship with mass diffusivity.

The impact of constructive/destructive chemical reaction rate on $\phi(\eta)$ is explicitly shown in Figure 16. Regarding constructive chemical reaction ($k < 0$), $\phi(\eta)$ rises with augmenting (absolute) values of the reaction rate parameter, but for destructive chemical reaction ($k > 0$), the opposite trend is noticed, i.e., $\phi(\eta)$ declines with augmenting k. "In other words, the reaction-rate parameter is a decelerating agent. This is due to the fact that the conversion of the species takes place as a result of chemical reaction and thereby reduces the concentration in the boundary-layer."

Figures 17 and 18 demonstrates the striking effect of A on $f'(\eta)$ and $\theta(\eta)$ respectively. The velocity slip primarily decelerates the fluid motion that implicitly substantiates a depletion in the net movement of the fluid molecules. Hence, amplifying values of A causes the fluid's velocity to diminish. Towards the full slip i.e., as $A \to \infty$, the frictional resistance between the viscous fluid and the sheet gets eradicated. Moreover, the sheet's stretching does no longer obtrude any fluid motion. This in turn upsurges the temperature distribution for various A.

The striking impact of Biot number on $\theta(\eta)$ is illustrated in Figure 19. At any location, the parameter Bi is directly proportional to h_f. Thus "as expected, the stronger convection results in higher surface temperatures, causing the thermal effect to penetrate deeper into the quiescent fluid". The temperature upsurges with increasing Bi. "It is found that the fluid temperature is linear in the absence of the Biot number, and an increase of the Biot number, increases the

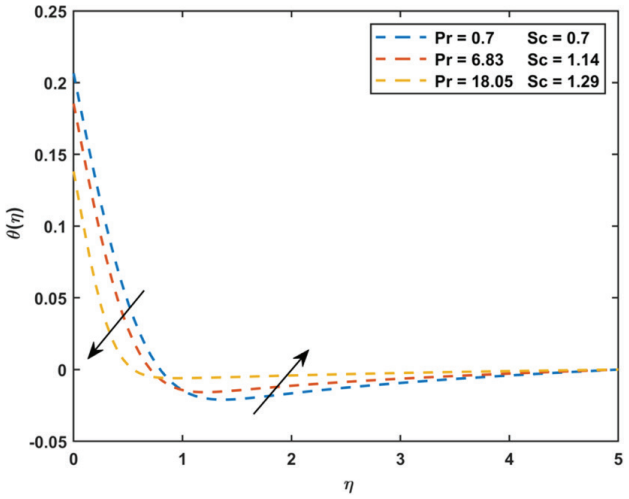

Figure 14. Temperature distribution for various *Pr* and *Sc*.

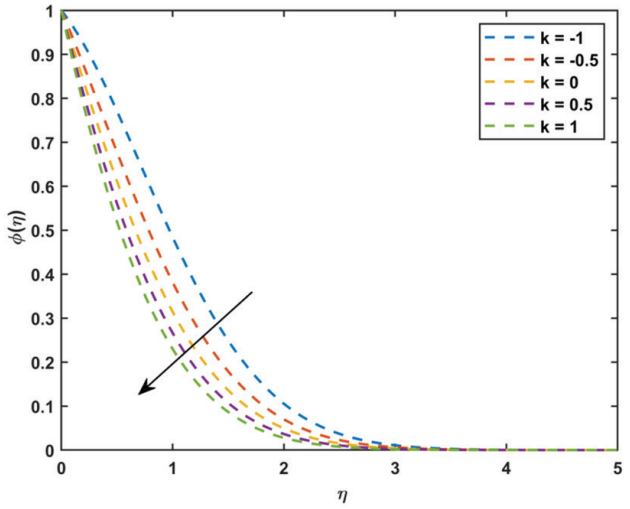

Figure 16. Concentration distribution for various *k*.

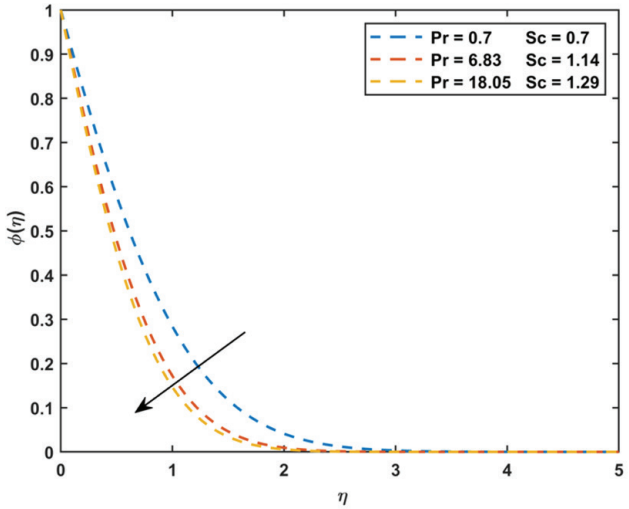

Figure 15. Concentration distribution for various *Pr* and *Sc*.

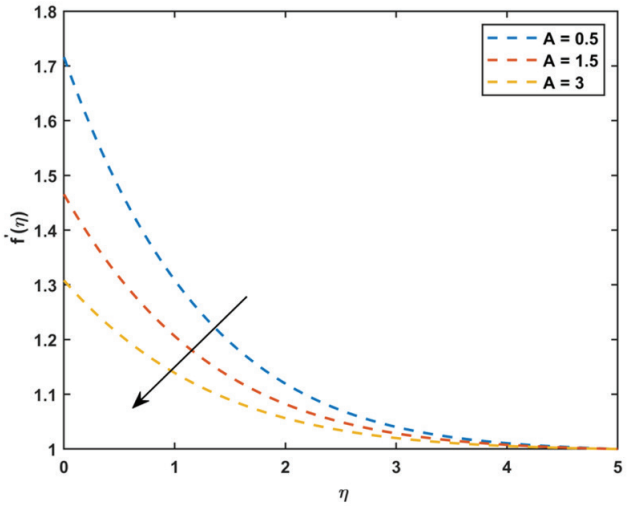

Figure 17. Velocity profile for various *A*.

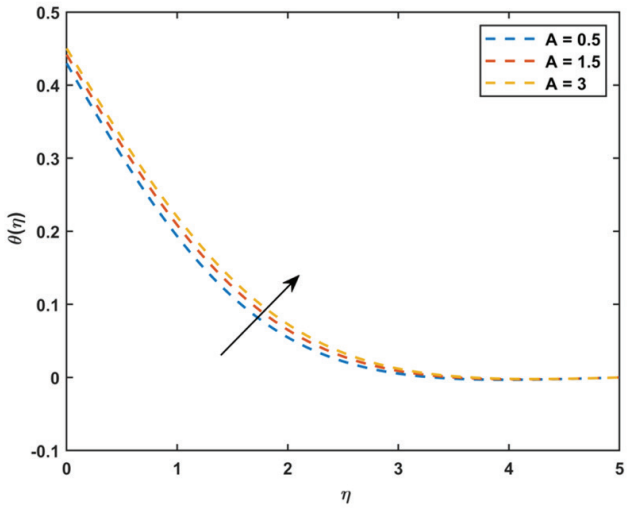

Figure 18. Temperature distribution for various *A*.

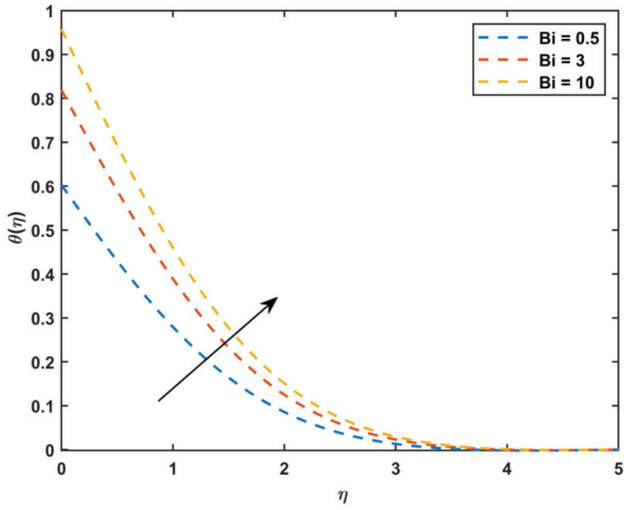

Figure 19. Temperature distribution for various *Bi*.

fluid temperature and thermal boundary layer thickness." As *Bi* goes to infinity, the boundary condition (20) reduces to $\theta(0) \to 1$ as $Bi \to \infty$. Hence, it is evident that the solution is anticipated to approach the classical solution of constant surface temperature problem.

CONCLUSION

The synergy of "variable thermal conductivity" and "non-uniform heat source/sink" on the stagnation point flow of Casson fluid past a convective stretching sheet, together with constructive/destructive reactions are inspected. The ODEs corresponding to the governing PDEs are deduced by virtue of a well-suited similarity transformation. bvp4c, an in-built technique of MATLAB is exerted to acquire the numerical solutions. "The impacts of multifarious dimensionless parameters on velocity profile, temperature and concentration distributions are illustrated graphically. The effect of involved parameters on skin friction coefficient, Nusselt number and Sherwood number are tabulated." The paramount findings of this evaluation are summed up as follows:

1. For internal heat generation, an increase in variable thermal conductivity parameter reduces the temperature. But this is not the case for internal heat absorption. An enhancement in ε, diminishes the temperature near the wall and as the fluid moves far away, the temperature distribution skyrockets.
2. The temperature-dependent and space-dependent internal heat absorption/generation (non-uniform heat sink/source) parameter augments the temperature distribution.
3. A simultaneous increase in Prandtl number and Schmidt number diminishes the temperature near the wall. But on the contrary, the temperature augments far away from the wall.
4. An amplification in the velocity slip, Casson parameter and magnetic field parameter reduces the fluid velocity. Moreover, the friction factor gets enhanced with rising values of velocity slip and Casson fluid parameter.
5. Augmenting Eckert number, thermal radiation and Biot number escalates the temperature distribution. The heat transfer skyrockets with rising Biot number and diminishes with increasing Eckert number and thermal radiation parameter.
6. The concentration distribution gets declined with a rise in velocity ratio parameter, Schmidt number and Prandtl number, and destructive chemical reaction. There is an escalation of mass transfer with intensification of the velocity ratio parameter, and the Sherwood number gets reduced with augmentation of the Casson fluid parameter.
7. For constant thermal conductivity with homogenous chemical reactions and in the absence of non-uniform heat source/sink, the outcomes are identical to those of [47].

Though the essentiality of variable thermal conductivity in the lunar soft lander technology serves as a potential application in the field of the aerospace industry, it is very significant to highlight a few limitations regarding this research work. Such limitations will not only help researchers analyse this work but also provide insights to extend it. In order to add an outlook and some future directions to the present work, one can study entropy generation, Soret-Dufour effects, or consider the three-dimensional investigation for the same geometry.

NOMENCLATURE

a, c	positive constants
x, y	Cartesian coordinates
τ_{ij}	$(i,j)^{th}$ component of stress tensor
B	Magnetic field intensity (*Tesla*)

T_f Temperature of hot fluid (K)
u Velocity component in the x direction (ms^{-1})
v Velocity component in the y direction (ms^{-1})
D Coefficient of mass diffusivity
T Temperature (K)
C Concentration (kgm^{-3})
C_w Surface concentration
C_∞ Ambient fluid concentration
T_∞ Ambient fluid temperature
K_w Surface thermal conductivity
K_∞ Free stream conductivity of the fluid
L Velocity slip
f Dimensionless stream function
M Magnetic field parameter
N Radiation parameter
α velocity ratio parameter
Ec Eckert number
Pr Prandtl number
Sc Schmidt number
k Reaction rate parameter
A Dimensionless velocity slip parameter
Bi Biot number
C_{fx} Skin friction coefficient
Nu_x Local Nusselt number
Sh_x Local Sherwood number

Greek symbols
μ Dynamic viscosity ($kgm^{-1}s^{-1}$)
β Casson fluid parameter
ν Kinematic viscosity (m^2s^{-1})
ρ Density (kgm^{-3})
c_p Specific heat capacity at constant pressure ($Jkg^{-1}K^{-1}$)
σ Electrical conductivity
ψ Stream function
η Similarity variable
θ Dimensionless temperature
ϕ Dimensionless concentration

AUTHORSHIP CONTRIBUTIONS

Authors equally contributed to this work.

DATA AVAILABILITY STATEMENT

The authors confirm that the data that supports the findings of this study are available within the article. Raw data that support the finding of this study are available from the corresponding author, upon reasonable request.

CONFLICT OF INTEREST

The authors declared no potential conflicts of interest with respect to the research, authorship, and/or publication of this article.

ETHICS

There are no ethical issues with the publication of this manuscript.

REFERENCES

[1] Crane LJ. Flow past a stretching plate. Z Angew Math Phys 1970;21:645–647. [CrossRef]
[2] Chiam TC. Stagnation-point flow towards a stretching plate. J Phys Soc Jpn 1994;63:2443. [CrossRef]
[3] Kumaran V, Ramanaiah G. A note on the flow over a stretching sheet. Acta Mech 1996;116:BF01171433. [CrossRef]
[4] Raptis A. Radiation and free convection flow through a porous medium. Int Commun Heat Mass Transf 1998;25:00016-5. [CrossRef]
[5] Andersson HI. Slip flow past a stretching surface. Acta Mech 2002;158:BF01463174. [CrossRef]
[6] Mahapatra TR, Gupta AS. Heat transfer in stagnation-point flow towards a stretching sheet. Heat Mass Transf 2002;38:s002310100215. [CrossRef]
[7] Paullet J, Weidman P. Analysis of stagnation point flow toward a stretching sheet. Int J Non Linear Mech 2007;42:003. [CrossRef]
[8] Wang CY. Stagnation flow towards a shrinking sheet. Int J Non Linear Mech 2008;43:021. [CrossRef]
[9] Tirth V, Pasha AA, Tayebi T, Dogonchi AS, Irshad K, Chamkha AJ, et al. Magneto double-diffusive free convection inside a C-shaped nanofluid-filled enclosure including heat and solutal source block. Case Stud Therm Eng 2023;45:102942. [CrossRef]
[10] Ishak A, Jafar K, Nazar R, Pop I. MHD stagnation point flow towards a stretching sheet. Phys A 2009;388:026. [CrossRef]
[11] Misra JC, Sinha A, Mallick B. Stagnation point flow and heat transfer on a thin porous sheet: Applications to flow dynamics of the circulatory system. Phys A 2017;470:051. [CrossRef]
[12] Agbaje TM, Mondal S, Makukula ZG, Motsa SS, Sibanda P. A new numerical approach to MHD stagnation point flow and heat transfer towards a stretching sheet. Ain Shams Eng J 2016;9:015. [CrossRef]
[13] Ghasemi SE, Hatami M. Solar radiation effects on MHD stagnation point flow and heat transfer of a nanofluid over a stretching sheet. Case Stud Therm Eng 2021;25:100898. [CrossRef]
[14] Zangooee MR, Hosseinzadeh K, Ganji DD. Hydrothermal analysis of hybrid nanofluid flow on a vertical plate by considering slip condition. Theor Appl Mech Lett 2022;12:100357. [CrossRef]
[15] Leng Y, Li S, Algarni S, Jamshed W, Alqahtani T, Ibrahim RW, et al. Computational study of magnetized and dual stratified effects on Non-Darcy Casson nanofluid flow: An activation energy analysis. Case Stud Therm Eng 2024;53:103804. [CrossRef]

[16] Mustafa M, Hayat T, Pop I, Hendi A. Stagnation-point flow and heat transfer of a Casson fluid towards a stretching sheet. Z Naturforsch A 2012;67:0057. [CrossRef]
[17] Bhattacharyya K. Boundary layer stagnation-point flow of Casson fluid and heat transfer towards a shrinking/stretching sheet. Front Heat Mass Transf 2013;4:3003. [CrossRef]
[18] Mukhopadhyay S, Bhattacharyya K, Hayat T. Exact solutions for the flow of Casson fluid over a stretching surface with transpiration and heat transfer effects. Chin Phys B 2013;22:114701. [CrossRef]
[19] Bhattacharyya K, Hayat T, Alsaedi A. Exact solution for boundary layer flow of Casson fluid over a permeable stretching/shrinking sheet. Z Angew Math Mech 2014;94:201200031. [CrossRef]
[20] Bhattacharyya K. MHD stagnation-point flow of Casson fluid and heat transfer over a stretching sheet with thermal radiation. J Thermodyn 2013;1:169674. [CrossRef]
[21] Kameswaran PK, Shaw S, Sibanda P. Dual solutions of Casson fluid flow over a stretching or shrinking sheet. Sadhana 2014;39:0289-7. [CrossRef]
[22] Lund LA, Omar Z, Khan I, Baleanu D, Nisar KS. Dual similarity solutions of MHD stagnation point flow of Casson fluid with effect of thermal radiation and viscous dissipation: stability analysis. Sci Rep 2020;10:72266-2. [CrossRef]
[23] Pashikanti J, Susmitha Priyadharshini DR. Influence of variable viscosity on entropy generation analysis due to graphene oxide nanofluid flow. J Nanofluids 2023;12:2026. [CrossRef]
[24] Kays WM, Crawford ME. Convective heat and mass transfer. 3rd ed. New York: McGraw Hill; 1993.
[25] Srinivasacharya D, Jagadeeshwar P. Effect of variable viscosity, thermal conductivity, and hall currents on the flow over an exponentially stretching sheet with heat generation/absorption. Int J Energy Clean Environ 2018;19:2018021746. [CrossRef]
[26] Arunachalam M, Rajappa NR. Thermal boundary layer in liquid metals with variable thermal conductivity. Appl Sci Res 1978;34:BF00418866. [CrossRef]
[27] Chiam TC. Heat transfer with variable conductivity in a stagnation-point flow towards a stretching sheet. Int Commun Heat Mass Transf 1996;23:00009-7. [CrossRef]
[28] Chiam TC. Heat transfer in a fluid with variable thermal conductivity over a linearly stretching sheet. Acta Mech 1998;129:BF01379650. [CrossRef]
[29] Sharma PR, Singh G. Effects of variable thermal conductivity and heat source/sink on MHD flow near a stagnation point on a linearly stretching sheet. J Appl Fluid Mech 2009;2:11851. [CrossRef]
[30] Venkateswarlu B, Satya Narayana PV. Influence of variable thermal conductivity on MHD Casson fluid flow over a stretching sheet with viscous dissipation, Soret and Dufour effects. Front Heat Mass Transf 2016;7:hmt.7.16. [CrossRef]
[31] Yu D-Y, Sun Z-Z, Zhang H. Thermal control technology of lunar lander. Technology of Lunar Soft Lander 2021:6580-9_5. [CrossRef]
[32] Dhange MY, Sankad GC, Maharudrappa I. Casson fluid flow due to stretching sheet with magnetic effect and variable thermal conductivity. Front Heat Mass Transf 2022;18:hmt.18.36. [CrossRef]
[33] Zangooee MR, Hosseinzadeh K, Ganji DD. Hydrothermal analysis of Ag and CuO hybrid NPs suspended in mixture of water 20%+EG 80% between two concentric cylinders. Case Stud Therm Eng 2023;50:103398. [CrossRef]
[34] Hussein AK, Hamzah HK, Ali FH, Kolsi L. Mixed convection in a trapezoidal enclosure filled with two layers of nanofluid and porous media with a rotating circular cylinder and a sinusoidal bottom wall. J Therm Anal Calorim 2020;141:08963-6. [CrossRef]
[35] Ali B, Khan SA, Hussein AK, Thumma T, Hussain S. Hybrid nanofluids: Significance of gravity modulation, heat source/sink, and magnetohydrodynamic on dynamics of micropolar fluid over an inclined surface via finite element simulation. Appl Math Comput 2022;419:126878. [CrossRef]
[36] Abo-Eldahab EM, El Aziz MA. Blowing/suction effect on hydromagnetic heat transfer by mixed convection from an inclined continuously stretching surface with internal heat generation/absorption. Int J Therm Sci 2004;43:005. [CrossRef]
[37] Abel MS, Mahesha N. Heat transfer in MHD viscoelastic fluid flow over a stretching sheet with variable thermal conductivity, non-uniform heat source and radiation. Appl Math Model 2008;32:038. [CrossRef]
[38] Monica M, Sucharitha J. Effects of nonlinear thermal radiation, non-uniform heat source/sink on MHD stagnation point flow of a Casson fluid over a nonlinear stretching sheet with slip conditions. J Nanofluids 2017;6:1360. [CrossRef]
[39] Li YX, Israr Ur Rehman M, Huang WH, Ijaz Khan M, Ullah Khan S, Chinram R, et al. Dynamics of Casson nanoparticles with non-uniform heat source/sink: A numerical analysis. Ain Shams Eng J 2022;13:010. [CrossRef]
[40] Ali MM, Chen TS, Armaly BF. Natural convection-radiation interaction in boundary-layer flow over horizontal surfaces. AIAA J 1984;22:8854. [CrossRef]
[41] Aziz A. A similarity solution for laminar thermal boundary layer over a flat plate with a convective surface boundary condition. Commun Nonlinear Sci Numer Simul 2009;14:003. [CrossRef]
[42] Ishak A. Similarity solutions for flow and heat transfer over a permeable surface with convective boundary condition. Appl Math Comput 2010;217:026. [CrossRef]

[43] Makinde OD, Aziz A. Boundary layer flow of a nanofluid past a stretching sheet with a convective boundary condition. Int J Therm Sci 2011;50:019. [CrossRef]
[44] Yao S, Fang T, Zhong Y. Heat transfer of a generalized stretching/shrinking wall problem with convective boundary conditions. Commun Nonlinear Sci Numer Simul 2011;16:028. [CrossRef]
[45] Mohamed MKA, Salleh MZ, Nazar R, Ishak A. Numerical investigation of stagnation point flow over a stretching sheet with convective boundary conditions. Bound Value Probl 2013:2013-4. [CrossRef]
[46] Raza J. Thermal radiation and slip effects on magnetohydrodynamic (MHD) stagnation point flow of Casson fluid over a convective stretching sheet. Propuls Power Res 2019;8:004. [CrossRef]
[47] Dessie H. MHD stagnation point flow of Casson fluid over a convective stretching sheet considering thermal radiation, slip condition, and viscous dissipation. Heat Transf 2021;50:22213. [CrossRef]
[48] Raghunath K, Ramana RM, Reddy VR, Obulesu M. Diffusion thermo and chemical reaction effects on magnetohydrodynamic Jeffrey nanofluid over an inclined vertical plate in the presence of radiation absorption and constant heat source. J Nanofluids 2022;12:1923. [CrossRef]
[49] Li S, Raghunath K, Alfaleh A, Ali F, Zaib A, Khan MI, et al. Effects of activation energy and chemical reaction on unsteady MHD dissipative Darcy–Forchheimer squeezed flow of Casson fluid over horizontal channel. Sci Rep 2023;13:29702-w. [CrossRef]
[50] Andersson HI, Hansen OR, Holmedal B. Diffusion of a chemically reactive species from a stretching sheet. Int J Heat Mass Transf 1994;37:90137-6. [CrossRef]
[51] Vajravelu K, Prasad KV, Prasanna Rao NS. Diffusion of a chemically reactive species of a power-law fluid past a stretching surface. Comput Math Appl 2011;62:055. [CrossRef]
[52] Bhattacharyya K, Uddin MS, Layek GC, Pk WA. Diffusion of chemically reactive species in boundary layer flow over a porous plate in porous medium. Chem Eng Commun 2013;200:762509. [CrossRef]
[53] Mukhopadhyay S, Vajravelu K. Diffusion of chemically reactive species in Casson fluid flow over an unsteady permeable stretching surface. J Hydrodyn 2013;25:60400-X. [CrossRef]
[54] Abbas Z, Javed T, Ali N, Sajid M. Diffusion of chemically reactive species in stagnation-point flow of a third-grade fluid: A hybrid numerical method. J Appl Fluid Mech 2016;9:24004. [CrossRef]
[55] Jena S, Dash GC, Mishra SR. Chemical reaction effect on MHD viscoelastic fluid flow over a vertical stretching sheet with heat source/sink. Ain Shams Eng J 2018;9:014. [CrossRef]
[56] Khan N, Al-Khaled K, Khan A, Hashmi MS, Khan SU, Khan MI, et al. Aspects of constructive/destructive chemical reactions for viscous fluid flow between deformable wall channel with absorption and generation features. Int Commun Heat Mass Transf 2021;120:104956. [CrossRef]
[57] Kanafiah SFHM, Kasim ARM, Zokri S, Arifin NS. A thematic review on mathematical model for convective boundary layer flow. J Adv Res Fluid Mech Therm Sci 2021;86:107125. [CrossRef]
[58] Brewster MQ. Thermal radiative transfer and properties. New York: Wiley; 1992.
[59] Verma VK, Mondal S. A brief review of numerical methods for heat and mass transfer of Casson fluids. Partial Differ Equ Appl Math 2021;3:100034. [CrossRef]
[60] Shampine LF, Gladwell I, Thompson S. Solving ODEs with MATLAB. Cambridge: Cambridge University Press; 2003. [CrossRef]
[61] Schlichting H, Gersten K. Boundary-Layer Theory. New York: Springer; 2016. [CrossRef]